J. Sens. Sens. Syst., 5, 147–156, 2016
www.j-sens-sens-syst.net/5/147/2016/
doi:10.5194/jsss-5-147-2016

JSSS Journal of Sensors and Sensor Systems Open Access

Selective detection of naphthalene with nanostructured WO_3 gas sensors prepared by pulsed laser deposition

Martin Leidinger[1], Joni Huotari[2], Tilman Sauerwald[1], Jyrki Lappalainen[2], and Andreas Schütze[1]

[1]Saarland University, Lab for Measurement Technology, Saarbrücken, Germany
[2]University of Oulu, Faculty of Information Technology and Electrical Engineering, Oulu, Finland

Correspondence to: Martin Leidinger (m.leidinger@lmt.uni-saarland.de)

Received: 15 October 2015 – Revised: 22 March 2016 – Accepted: 28 March 2016 – Published: 8 April 2016

Abstract. Pulsed laser deposition (PLD) at room temperature with a nanosecond laser was used to prepare WO_3 layers on both MEMS microheater platforms and Si/SiO_2 substrates. Structural characterization showed that the layers are formed of nanoparticles and nanoparticle agglomerates. Two types of layers were prepared, one at an oxygen partial pressure of 0.08 mbar and one at 0.2 mbar. The layer structure and the related gas sensing properties were shown to be highly dependent on this deposition parameter. At an oxygen pressure of 0.2 mbar, formation of ε-phase WO_3 was found, which is possibly contributing to the observed increase in sensitivity of the sensor material.

The gas sensing performance of the two sensor layers prepared via PLD was tested for detection of volatile organic compounds (benzene, formaldehyde and naphthalene) at ppb level concentrations, with various ethanol backgrounds (0.5 and 2 ppm) and gas humidities (30, 50 and 70 % RH). The gas sensors were operated in temperature cycled operation. For signal processing, linear discriminant analysis was performed using features extracted from the conductance signals during temperature variations as input data.

Both WO_3 sensor layers showed high sensitivity and selectivity to naphthalene compared to the other target gases. Of the two layers, the one prepared at higher oxygen partial pressure showed higher sensitivity and stability resulting in better discrimination of the gases and of different naphthalene concentrations. Naphthalene at concentrations down to 1 ppb could be detected with high reliability, even in an ethanol background of up to 2 ppm. The sensors show only low response to ethanol, which can be compensated reliably during the signal processing. Quantification of ppb level naphthalene concentrations was also possible with a high success rate of more than 99 % as shown by leave-one-out cross validation.

1 Introduction

In order to evaluate and assess indoor air quality (IAQ), different types of gaseous chemical compounds have to be considered. In addition to carbon monoxide (CO), carbon dioxide (CO_2) and nitrogen dioxide (NO_2), low concentrations of volatile organic compounds (VOCs) play a significant role in deteriorating the quality of breathing air in buildings (World Health Organization, 2010; Bernstein et al., 2008). Exposure to these substances, even at low concentrations, can lead to severe negative effects on human health. For VOCs, health problems mainly include damage to the respiratory system and skin irritations (Jones, 1999). Additionally, some VOCs are proven to be carcinogenic (e.g., benzene, World Health Organization, 2010) or are suspected to be carcinogenic (e.g., formaldehyde, Guo et al., 2004). Based on toxicity and prevalence, according to the World Health Organization (WHO) and the INDEX project (Koistinen et al., 2008), the highest priority VOCs for IAQ are formaldehyde, benzene and naphthalene. For naphthalene, the WHO guidelines suggest values below 0.01 mg m^{-3} corresponding to 1.9 ppb (World Health Organization, 2010). The main health concerns for naphthalene are lesions in the respiratory tract, including tumors in the upper airways (World Health Organization, 2010).

In order to detect such small concentrations of VOCs without the need for expensive and time-consuming analytical measurements (e.g., GC-MS analysis, Wu et al., 2004), metal oxide semiconductor gas sensors can be applied. Detection of VOCs in the ppb range with such sensors has been successfully demonstrated using temperature cycled operation (TCO) and pattern recognition signal processing with ceramic-based thick film sensors (Leidinger et al., 2014); however, significant cross-sensitivity to ethanol was found mainly for SnO_2-based sensors. In order to reduce this cross-sensitivity, WO_3 layers were investigated. To obtain highly sensitive sensors with small thermal time constants, the MOS thin film layers were produced on microheater substrates by pulsed laser deposition (PLD). We found that these sensors show a high response to naphthalene in the relevant concentration range with high selectivity compared to other gases, especially relevant interferent gases for indoor air quality assessment, e.g., ethanol.

Pulsed laser deposition is a method for depositing a variety of materials ranging from epitaxial thin films (Hussain et al., 2005) to highly porous nanostructured layers (Balandeh et al., 2015). Porous nanostructured layers have been studied especially in the context of gas sensing materials (Caricato et al., 2009; Nam et al., 2006). PLD offers many advantages compared to other deposition methods, for example easily controllable film composition by deposition parameters, and a good repetition of stoichiometry of the target material in the films deposited on the substrate. When using nanosecond laser PLD, as in this study, with a high oxygen partial pressure in the deposition chamber, nanoparticle formation starts during the deposition process leading to a highly porous nanostructured layer (Harilal et al., 2003; Infortuna et al., 2008; Huotari et al., 2015). These types of layers are very suitable for gas sensing purposes because of their high specific surface area.

WO_3 as a material has been widely studied as it offers a large range of possibilities in practical applications, e.g., in gas sensing (Kohl et al., 2000; Wang et al., 2008; Balazsi et al., 2008), and photocatalytic water splitting (Pihosh et al., 2015). There are several methods to produce WO_3 layers ranging from thick film and thin films technologies to chemical methods (Zheng et al., 2011). In this study, PLD was utilized for depositing WO_3 layers on MEMS microhotplates to produce low-cost and high-performance gas sensor devices.

The performance of the PLD sensor layers has been evaluated in test gas measurements. The three high-priority VOCs, benzene, formaldehyde and naphthalene, have been applied in concentrations below, at and above the respective guideline values, and ethanol has been added as an interferent gas in much higher concentrations in order to simulate typical IAQ applications with background gases from, e.g., cleaning agents or alcoholic beverages. The sensors were operated in dynamic operation using temperature cycled operation (TCO), which is a well-known method for increasing sensitivity and selectivity of gas sensor systems based on MOS sensors (Heilig et al., 1997; Lee and Ready, 1999; Paczkowski et al., 2013; Baur et al., 2014). The resulting signals, after pre-processing and feature extraction, were analyzed by linear discriminant analysis (LDA), a multivariate pattern recognition method which separates different classes of input data while trying to group data sets of the same assigned group (Klecka, 1980; Gutierrez-Osuna, 2002). The combination of TCO and LDA has shown to improve selectivity and sensitivity of gas sensors, both MOS sensors (Gramm et al., 2003; Meier et al., 2007; Reimann and Schütze, 2012; Leidinger et al., 2014) and other types, e.g., GasFET devices (Bur et al., 2012).

2 PLD sensor layer deposition and characterization

2.1 Sensor layer deposition

A XeCl laser with a wavelength of $\lambda = 308$ nm was used to produce WO_3 layers on both Si/SiO_2 substrates and commercial microheater MEMS platforms from a ceramic WO_3 pellet. The laser pulse length was 25 ns and pulse fluence was $I = 1.25\,J\,cm^{-2}$. In all depositions the substrate temperature was kept at room temperature (RT). Two types of samples have been prepared, one at a low O_2 partial pressures of $p(O_2) = 0.08$ mbar, designation PLD0.08O2, and a second type with a higher partial pressure of $p(O_2) = 0.2$ mbar, designation PLD0.2O2. All samples were annealed in a furnace at 400 °C for 1 h after deposition. The samples deposited on Si/SiO_2 substrates were used as reference samples in structural characterization of the layers, and samples with the MEMS heaters were used in gas sensing measurements.

A Bruker D8 Discover device was used in X-ray diffraction studies, and Raman spectroscopy studies were performed with a HORIBA Jobin Yvon LabRAM HR800 in order to study the crystal structure and symmetry of the layers. The surface morphology and the film composition of the samples were studied with a Veeco Dimension 3100 atomic force microscope (AFM) and with Zeiss Sigma FESEM device.

2.2 Crystal structure characterization of the sensing layers

The grazing incidence diffraction (GID) method of the X-ray diffraction was used to characterize the WO_3 layers annealed at 400 °C for 1 h. The results are shown in Fig. 1. A clear difference in the crystal structure can be seen. The phase composition of layers deposited at $p(O_2) = 0.08$ mbar is mostly of the monoclinic γ phase of WO_3, but in the samples deposited at $p(O_2) = 0.2$ mbar, also the ferroelectric monoclinic ε phase of WO_3 is present. This is emphasized especially by the (110) and (−112) reflections located at $2\theta \approx 24.0$ and 33.3°, respectively (Johansson, 2012). However, one must remember that the crystal structures of the

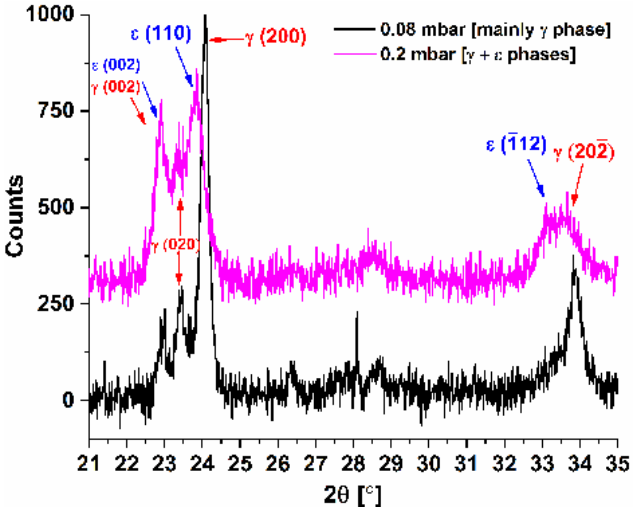

Figure 1. X-ray diffraction spectra of the deposited WO_3 layers after annealing in air (400 °C for 1 h).

γ phase and the ε phase are quite similar, and thus both of them have XRD reflections either in the same 2θ angels or very close to each other. The average grain size of both types of samples after annealing was determined to be around 30 nm using the Warren–Averbach method for XRD data (Marinkovic et al., 2001).

In Fig. 2, the Raman spectroscopy studies performed to the WO_3 layers are presented. The Raman spectra of the as-deposited samples immediately after deposition without any heat treatment are shown in Fig. 2a, and in Fig. 2b the spectra of the layers after annealing at 400 °C for 1 h are presented. An interesting property of the deposition process can be identified in the non-annealed samples. When the O_2 partial pressure is 0.08 mbar, the samples seem to be in an amorphous state after deposition, but when the O_2 pressure is 0.2 mbar, some crystallization is already evident during the deposition process at RT, even before any heat treatment to the layers. However, from Fig. 2b, showing the Raman spectra of the samples after the annealing process, it is clearly seen that after heat treatment in a furnace both films have a more crystallized structure. It is also again evident that the layers PLD0.08O2 are composed mostly of γ phase, but the samples PLD0.2O2 have also the ε phase in their crystal structure, verified from the Raman modes at wavenumbers 67, 97, 144, 183, 203, 272, 303, 370, 425, 644, and 680 cm^{-1} (Wang et al., 2008; Johansson et al., 2012; Souza Filho et al., 2000). Similarly as the reflections in XRD measurements, both γ phase and ε phase have Raman modes either at same wavenumbers or very close to each other.

At this point it should be noted that usually the ferroelectric ε phase only exists in temperatures below −40 °C. However, different studies (Wang et al., 2008; Righettoni et al., 2010; Johansson et al., 2012) show that the ε phase can exist in a solid-state form also at temperatures above RT. The

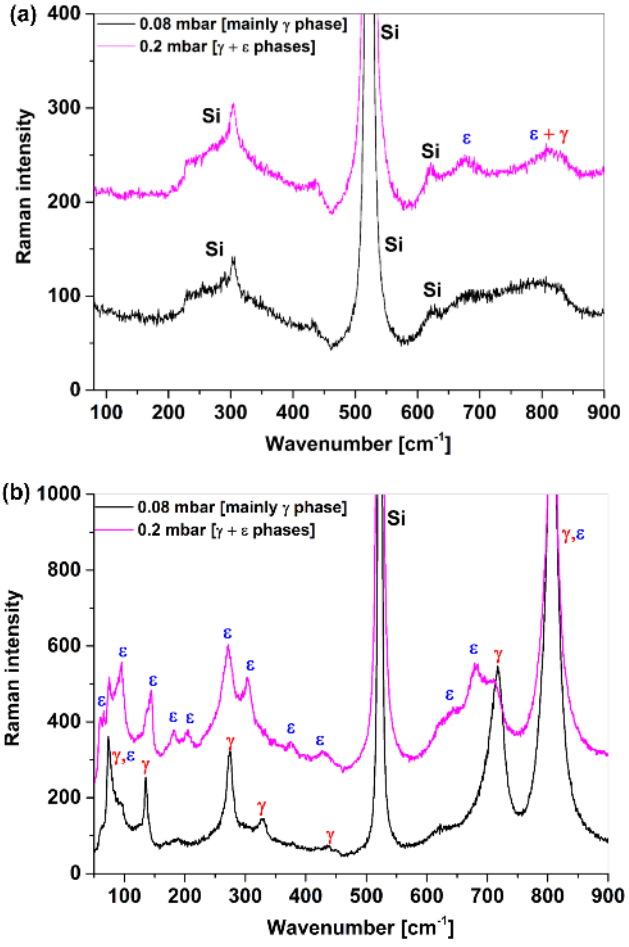

Figure 2. Raman spectra of the deposited WO_3 layers **(a)** as-deposited samples, **(b)** after annealing at 400 °C for 1 h.

reason for this is believed to be the small particle size of the samples, similarly as in the samples presented in this study. Also, the existence of the ε phase in the WO_3 composition has been proven to enhance WO_3 structures sensitivity to acetone (Wang et al., 2008; Righettoni et al., 2010; Sood and Gouma, 2013). The reason was suggested to be the ferroelectricity of the ε phase, namely the spontaneous electric dipole moments it possesses, which are then highly contributing to the chemical reaction between the WO_3 surface and the target gas.

2.3 Film composition characterization of the sensing layers

The surface morphology of the as-deposited and annealed WO_3 samples was studied by atomic force microscopy, and the results are shown in Fig. 3. The surface micrographs of the as-deposited layer and the annealed layer of sample PLD0.08O2 are shown in Fig. 3a and b, respectively. The sample surfaces consist of small agglomerates of nanopar-

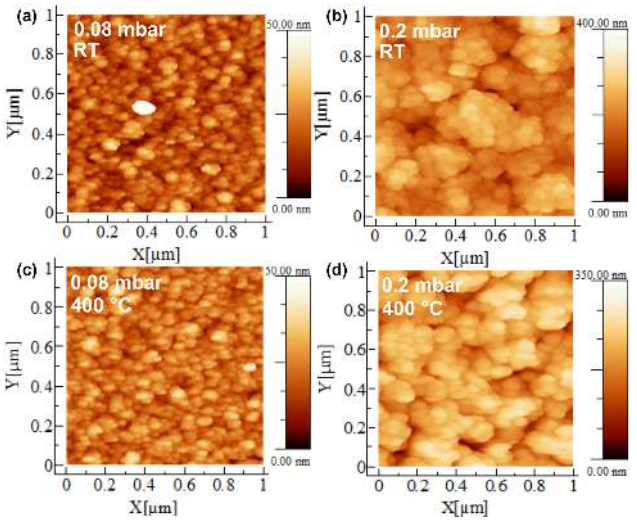

Figure 3. Atomic force microscopy surface micrographs of the deposited WO_3 layers showing the influence of oxygen partial pressure during deposition **(a, b)** as-deposited samples, **(c, d)** after annealing at 400 °C for 1 h.

ticles. In Fig. 3c and d, the surface micrographs of the as-deposited layer and the annealed layer of sample PLD0.2O2 are shown, respectively. The layers consist also of small nanoparticles, but agglomerated to bigger clusters. Also, the layer structure is much rougher and more porous than on the samples deposited at 0.08 mbar O_2. It can also be clearly seen that the annealing process at 400 °C for 1 h does not have a great effect on the surfaces of the samples. In both cases, the average surface roughness value R_q was the same before and after the annealing process, being $R_q = 5.5$ nm for sample PLD0.08O2, and $R_q = 42.2$ nm for sample PLD0.2O2. The crystallization, which is observed for the PLD0.08O2 sample seems to be a local process that does not involve larger-scale material transport.

Scanning electron microscopy was used to further study the film composition of the samples. Both surface micrographs and cross-section micrographs were taken from the samples. In Fig. 4a and b the cross-section micrograph and surface micrograph of the as-deposited sample fabricated at $p(O_2) = 0.08$ mbar are shown, respectively. The cross-section graph shows that the film is composed of small nanoparticle agglomerates formed as pillar-like structures, with some porosity in between the columns. The surface graph shows that the film surface is formed of small nanoparticle agglomerates and thus verifies the measurements made with AFM. The cross-section micrograph and surface micrograph of the as-deposited sample fabricated at $p(O_2) = 0.2$ mbar are shown in Fig. 4b and c, respectively. Now the film composition is much more porous and rough compared to the PLD0.08O2 film, and also the nanoparticle agglomerate size is larger. The agglomerates form clearer pillar-like morphology on top of the substrate. The surface of the film is

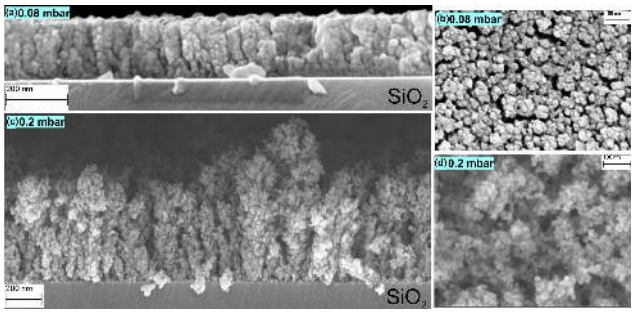

Figure 4. Scanning electron microscopy micrographs (cross sections and top views) of the as-deposited WO_3 layers deposited **(a, b)** at $p(O_2) = 0.08$ mbar, and **(c, d)** at $p(O_2) = 0.2$ mbar.

highly porous, concurrent with the AFM measurements performed.

3 Gas sensor performance

3.1 Gas test measurement setup

The gas sensing performance of the two sensor layers was evaluated in an extensive test measurement. The three target VOC gases were applied in three concentrations each, the middle concentrations representing the respective WHO guideline values of 0.1 mg m^{-3} (81 ppb) for formaldehyde and 0.01 mg m^{-3} (1.9 ppb) for naphthalene (World Health Organization, 2010), as well as the European Union guideline value of 5 µg m^{-3} (1.6 ppb) for benzene (European Parliament, Council of the European Union, 2008). Additionally, ethanol was introduced as a background gas in two concentrations, both much higher than the target gas concentrations. As the third varied parameter, the gas humidity was set in three steps. Table 1 shows all gases and concentrations.

The test gases were generated in a gas mixing system specifically designed for trace gases by Helwig et al. (2014). The gases were mixed into zero air produced by two cascaded zero air generators. Ethanol and formaldehyde test gases were taken from gas cylinders and diluted into the zero air carrier gas stream, either with a one-step dilution (ethanol) or a two-step dilution (formaldehyde). Benzene and naphthalene test gases were generated from permeation tubes in permeation ovens. Each target VOC concentration was set twice during each combination of humidity and ethanol background, first from highest to lowest concentration, then back to the highest concentration. The length of each VOC run was 30 min; between two trace VOC applications the sensors were purged with zero air with the respective ethanol and humidity configuration. In total, 90 different gas mixtures were generated and tested with the sensors; the total length of the measurement was 123 h.

For temperature cycled operation of the sensors, a ramp-up–ramp-down approach was chosen; the temperature of the microheaters was increased from 200 to 400 °C in 20 s and

Table 1. Test gas setup. Each gas concentration was applied at each EtOH background and humidity level for 30 min; between gas exposures sensors were exposed to background for 30 min.

Gas	Concentration (ppb)	EtOH background (ppm)	Humidity (% RH)
Zero air		0; 0.5; 2	30, 50, 70
Formaldehyde	200, 80, 40, 40, 80, 200	0; 0.5; 2	30, 50, 70
Benzene	2.5, 1.5, 0.5, 0.5, 1.5, 2.5	0; 0.5; 2	30, 50, 70
Naphthalene	5, 2, 1, 1, 2, 5	0; 0.5; 2	30, 50, 70

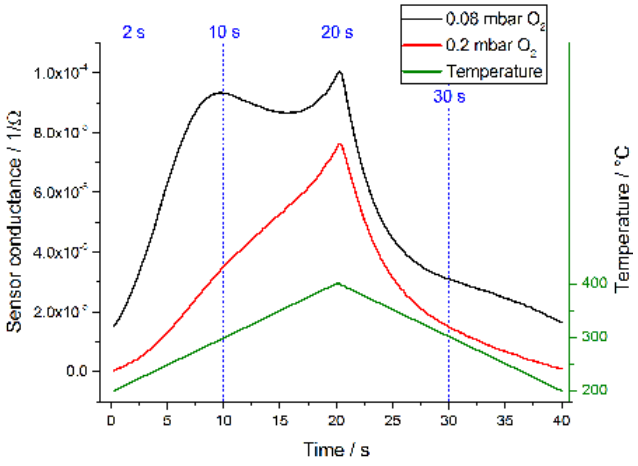

Figure 5. Gas sensor temperature cycle (green) and corresponding sensor signals of the two PLD WO_3 sensors in air at 30 % RH. The dashed lines indicate the selected points for quasi-static sensor signal analysis (cf. Fig. 6).

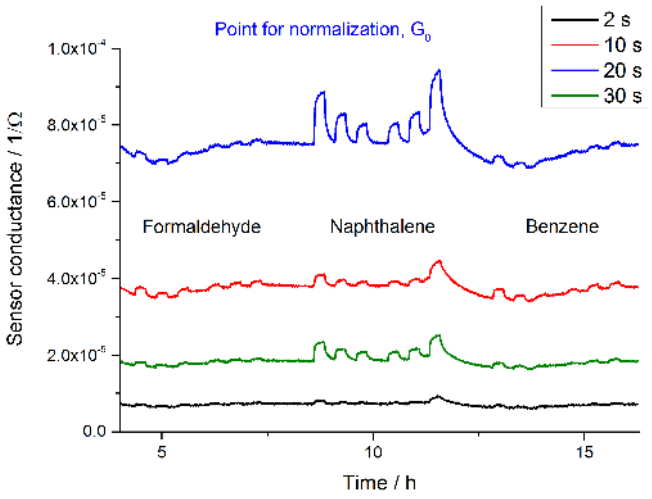

Figure 6. Quasi-static sensor signals for the four points indicated in Fig. 5 during exposure of the PLD0.2O2 sensor to formaldehyde, naphthalene and benzene at relevant ppb levels (Table 1) in air at 30 % RH without EtOH background. For later normalization, the value G_0 was extracted during background before the first exposure to naphthalene as indicated.

then reduced back to 200 °C in the same time, creating a 40 s cycle (see Fig. 5). The two sensor types clearly show differing behavior during the temperature cycle, especially during increase of the heater temperature.

3.2 Gas measurement results

For a first signal evaluation, quasi-static sensor signals were extracted from the raw sensor signal data sets. These signals were generated by plotting the signal value of certain points in the TCO cycle for each cycle, i.e., over the course of the complete measurement. An example of the PLD0.2O2 sensor is given in Fig. 6. Four points of the temperature cycle were selected, indicated in Fig. 5. A section of the measurement was chosen in which all three test VOCs are applied at 30 % RH gas humidity and without ethanol background. The sensor response to all concentrations of naphthalene is clearly visible, as well as the much lower responses to the other VOCs. By normalizing the signals, i.e., calculating the relative change of conductance G/G_0, the sensor response to naphthalene at the different points in the cycle can be determined (cf. Fig. 7). In this plot, it can be seen that the highest sensitivity, of the chosen points in the cycle, is during cooling of the sensor, 30 s after start of the cycle. The

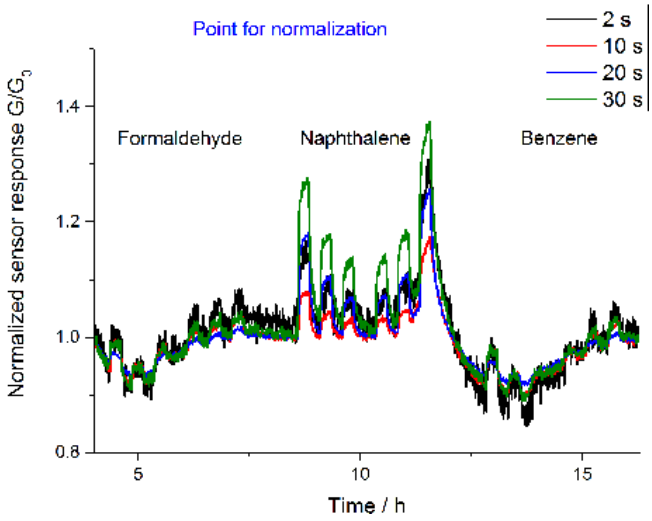

Figure 7. Normalized quasi-static signals for sensor PLD0.2O2 for the four selected points in the temperature cycle (cf. Fig. 5).

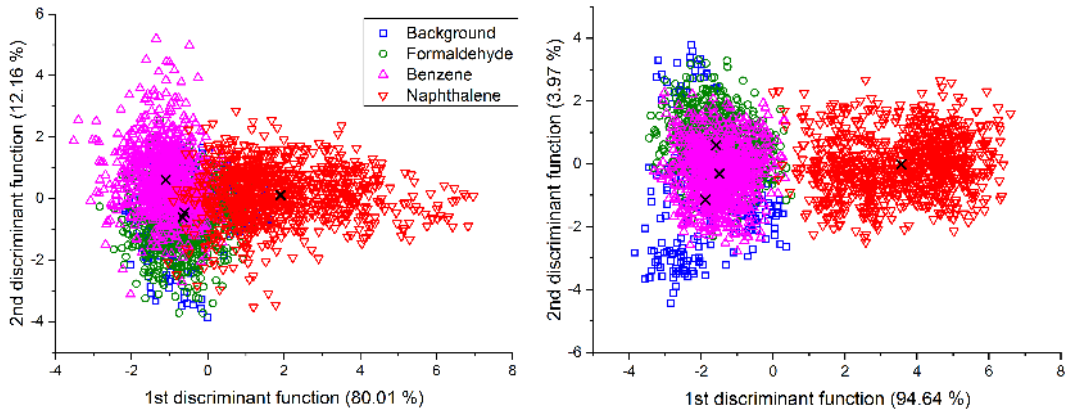

Figure 8. LDA plots for discrimination of different VOCs under varying humidity (30–70 % RH) and changing ethanol background (0–2 ppm), left: PLD0.08O2; right: PLD0.2O2.

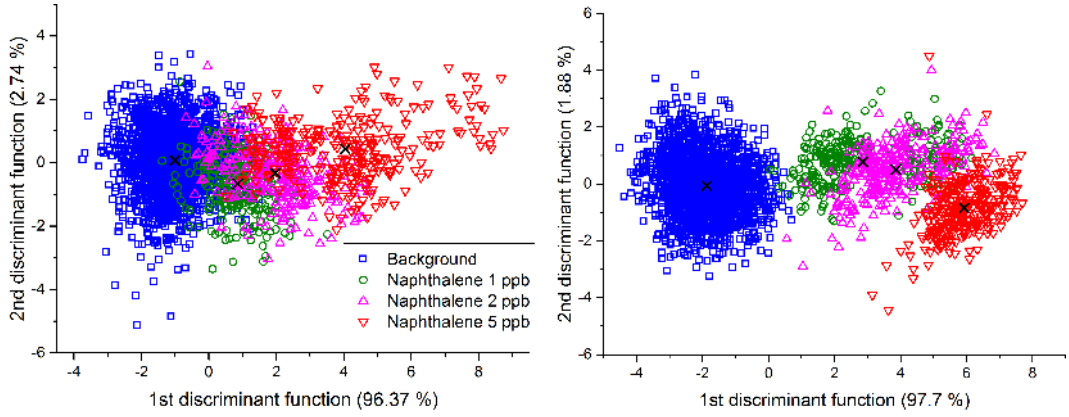

Figure 9. LDA plots for quantification of naphthalene under varying humidity (30–70 % RH) and changing ethanol background (0–2 ppm), left: PLD0.08O2; right: PLD0.2O2.

change of conductance is approx. 15 % for 1 ppb of naphthalene. The reason for the high selectivity to naphthalene is not known in detail and should be studied more closely. However, it was reported earlier that WO_3 has a specific response to aromatic compounds (Sauerwald, 2008) and that in general higher molecular weight leads to an increased sensitivity for this material (Sauerwald, 2008; Kohl et al., 2000).

The dynamic sensor signal patterns were analyzed using LDA. The whole procedure of generating data sets for LDA from dynamic gas sensor signals and the options for LDA application were described by Bur et al. (2014). As input data for each sensor, a limited number of features were extracted from the respective sensor signal of each temperature cycle. In this case, the cycle was divided into 20 segments of equal length (2 s). For each segment, the mean value and the slope of the sensor signal were calculated and used as features. This generates a feature vector with 40 values for each temperature cycle. These data sets were grouped into different groups, depending on the desired data analysis.

For the first analysis, the complete data set, containing 2799 feature vectors, was used as input data for the LDA. All cycles which contain a certain VOC were grouped together, regardless of VOC concentration, humidity and ethanol background. This results in one group for each target VOC and a "background" group, which contains the data sets of the TCO cycles which ran when no trace VOC was applied. This analysis checks the performance of the sensors to discriminate the target gases in varying humidity and background conditions. The LDA result plots for the two sensors with the PLD layers are shown in Fig. 8, left for the PLD0.08O2 sensor and right for the PLD0.2O2 type. For both sensors, the background, formaldehyde and benzene groups are overlapping strongly, while the naphthalene group is more separated. Especially for the PLD0.2O2 sensor the naphthalene group is nearly completely split from the other gases.

As a quantitative measure of the discrimination result, leave-one-out cross validation was performed on the data (LOOCV; Gutierrez-Osuna, 2002), with k nearest neighbors (kNN, $k = 5$) as classifier. This method calculates how many

Table 2. Leave-one-out cross-validation (LOOCV) results for all LDA investigations.

LDA no.	Analysis	PLD0.08O2	PLD0.2O2
1a	Gas discrimination (all gases)	66.5 %	71.9 %
1b	Gas discrimination (naphthalene)	86.3 %	99.2 %
2	Naphthalene quantification (full data set)	83.4 %	94.0 %
3	Naphthalene quantification (reduced data set, only 0 ppm EtOH background)	99.3 %	99.7 %
4	Humidity quantification	100 %	99.7 %
5a	Gas discrimination (all gases, only 50 % RH)	85.4 %	86.7 %
5b	Gas discrimination (naphthalene, only 50 % RH)	91.0 %	100 %

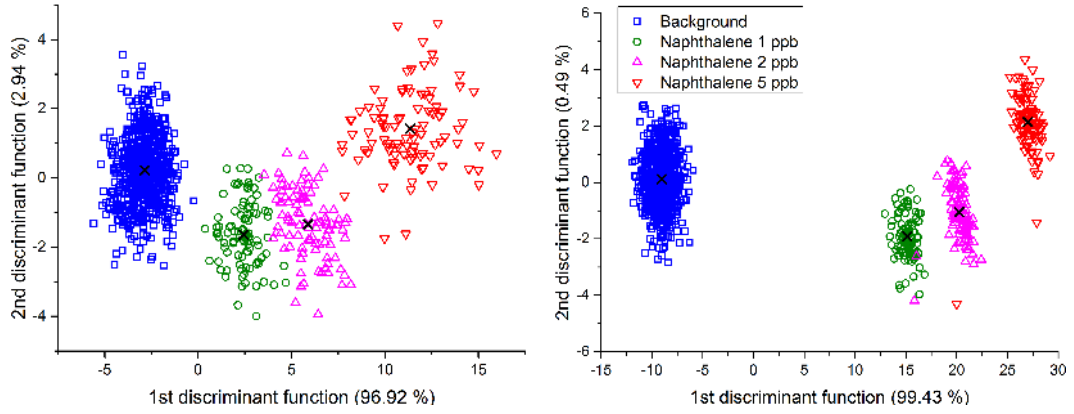

Figure 10. LDA plots for quantification of naphthalene under varying humidity (30–70 % RH) but with 0 ppm ethanol background, left: PLD0.08O2; right: PLD0.2O2.

feature vectors are classified correctly whether the LDA is trained by all other vectors.

Of the two sensors, the one with the PLD0.2O2 layer shows the better discrimination result overall, with 71.9 % correctly classified data points. The PLD0.08O2 achieves 66.5 %. The same order is given for classification of the naphthalene data points. The layer deposited at 0.2 mbar of O_2 shows a much better classification performance (99.2 % correct classifications) compared to the second sensor. The LOOCV results are summarized in Table 2, LDA 1a and 1b.

In the next step, it was checked if a quantification of the naphthalene concentration was possible. The full data set was used again. Each naphthalene concentration was assigned a group (with all humidities and ethanol backgrounds), and the other VOCs were assigned to the background group. The results for both tested sensors are plotted in Fig. 9. In this analysis, the PLD0.2O2 sensor shows the best separation of the groups again. There are some data points from the 1 ppb group located in the 2 ppb group. Otherwise, the three naphthalene concentrations are well lined up along the first discriminant axis. The PLD0.08O2 sensor shows less discrimination of the groups, which is also shown in LOOCV results (see Table 2, LDA 2).

The same analysis was attempted with a reduced data set, which included only the segments of the measurement without the ethanol background (950 sensor cycles in total). This significantly increases the quality of discrimination and thus naphthalene quantification for the sensors (see Fig. 10). Especially the PLD0.2O2 sensor has excellent separation of the naphthalene concentrations along the first discriminant function; the PLD0.08O2 sensor layer has much wider groups. The LOOCV results, listed in Table 2, LDA 3, show nearly 100 % correct classifications for the better sensor (PLD0.2O2); the second sensor layer also has over 99 % success rate.

Another evaluation of the sensor data was performed regarding quantification of gas humidity. The full data set was split into three groups, for the three gas humidities set during the measurement. This LDA run checks the sensors' cross-sensitivity to humidity, which also shows if the sensor would be able to measure the gas humidity. See Fig. 11 for the LDA result plots. These plots and the corresponding LOOCV results (Table 2, LDA 4) show very good discrimination of the humidities, which means that the sensor layers deposited by PLD have considerable sensitivity to water. However, this also means that the sensors could be used to measure the gas humidity or that the sensor performance could be monitored by comparing the predicted gas humidity with the value of a reference humidity sensor.

If the gas humidity is known, either from the gas sensor itself or from an additional humidity sensor, the quality of the signal processing can be improved by calculating different

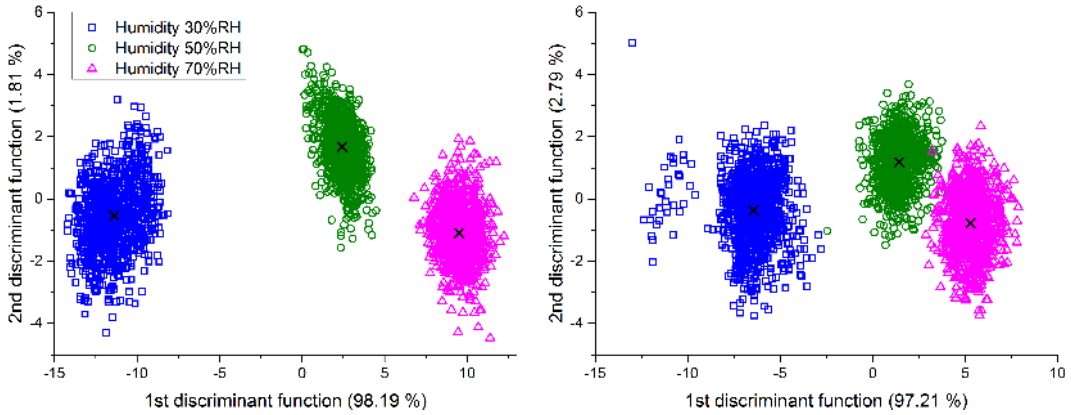

Figure 11. LDA plots for discrimination of ambient humidity levels for all sensor cycles with and without VOCs under varying ethanol background (0–2 ppm), left: PLD0.08O2; right: PLD0.2O2.

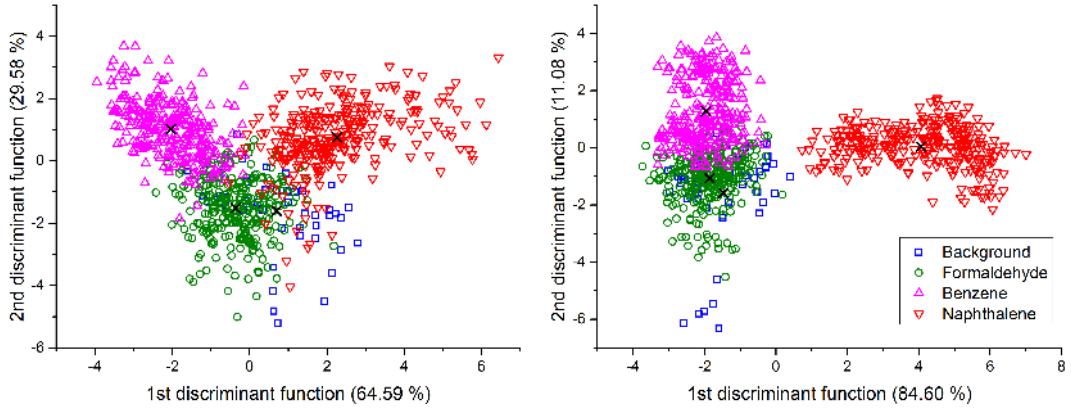

Figure 12. LDA plots for discrimination of different VOCs under constant humidity (50 % RH) and changing ethanol background (0–2 ppm), left: PLD0.08O2; right: PLD0.2O2.

LDA projections for several humidity ranges. A simple version of this approach has been tested by reducing the data set to the sensor signals acquired in one humidity, in this case all cycles measured in 50 % RH. The LDA result for gas identification for this is shown in Fig. 12. Compared to the full data set with three humidity levels (Fig. 8), the separation of the gases is clearly improved, especially for the PLD0.08O2 sensor. LOOCV also shows significant improvement of the classification results (Table 1, LDA 5). For all gases, the ratio of correct classifications was raised from 66.5 to 85.4 % for sensor PLD0.08O2 and from 71.9 to 86.7 % for sensor PLD0.2O2. For the naphthalene group, perfect classification was achieved for the sensor with 0.2 mbar O_2 partial pressure (Table 1, LDA 5b). A hierarchical data processing approach, which in the first step determines the humidity and in the second step classifies the gas, seems promising.

4 Conclusions

Nanoporous WO_3 gas sensing layers have successfully been prepared via nanosecond pulsed laser deposition, characterized, and tested for their gas sensing performance, especially for use in IAQ applications.

The characterization of the PLD sensing layers showed films formed of nanoparticle agglomerates with pillar-like morphology. The films were highly porous in their structure, especially when higher oxygen partial pressure was used during the deposition process. The crystal structure of the films was also dependent on the oxygen partial pressure with higher O_2 pressure resulting in the formation of $WO_3\varepsilon$ phase, which in bulk WO_3 samples is only stable at temperatures below −40 °C. The ε phase in the PLD films was observed to withstand annealing at 400 °C for 1 h probably due to its monocrystalline structure.

The two compared PLD sensor layer samples showed significant differences in their gas sensing performance. The layer deposited at higher oxygen partial pressure displayed improved response and excellent selectivity to naphthalene.

Both discrimination of different target VOCs and quantification of naphthalene were more successful with this sensor.

Naphthalene concentrations down to 1 ppb could be quantified with the sensor layer deposited at 0.2 mbar of O_2 with nearly 100 % success rate as determined by leave-one-out cross validation when no ethanol background was present. Even in varying ethanol background of up to 2 ppm, quantification was still successful for 94 % of all temperature cycles for this sensor. Detection of the presence of naphthalene in concentrations of 1 ppb or more had a success rate of more than 99 %, again determined by LOOCV.

The highly porous structure and possibly the formation of the WO_3 ε phase resulting from the higher oxygen pressure during PLD thus boost the gas sensing performance considerably. With the selected parameters, suitable gas sensing layers for detection and quantification of naphthalene have been obtained. Future investigations will address further improvement of the gas sensitive layers, e.g., by further variations of the deposition parameters as well as introduction of additional nanoparticles for doping and catalytic activation. We are also planning to study PLD deposition based on picosecond laser pulses which allows further optimization of the deposition parameters.

Acknowledgements. This project has received funding from the European Union's Seventh Framework Programme for research, technological development and demonstration under grant agreement no. 604311, Project SENSIndoor.

Edited by: M. Penza
Reviewed by: two anonymous referees

References

Balandeh, M., Mezzetti, A., Tacca, A., Leonardo, S., Marra, G., Divitini, G., Ducati, C., Medad, L., and Di Fonzo, F.: Quasi-1D hyperbranched WO_3 nanostructures for low-voltage photoelectrochemical water splitting, J. Mater. Chem. A, 3, 6110–6117, doi:10.1039/C4TA06786J, 2015.

Balazsi, C., Wang, L., Zayim, E. O., Szilagy, I. M., Sedlackov, K., Pfeifer, J., Toth, A. L., and Gouma, P.-I.: Nanosize hexagonal tungsten oxide for gas sensing applications, J. Eur. Ceram. Soc., 28, 913–917, doi:10.1016/j.jeurceramsoc.2007.09.001, 2008.

Baur, T., Schütze, A., and Sauerwald, T.: Optimierung des temperaturzyklischen Betriebs von Halbleitergassensoren, tm – Technisches Messen, 82, 187–195, doi:10.1515/teme-2014-0007, 2014.

Bernstein, J. A., Alexis, N., Bacchus, H., Leonard Bernstein, I., Fritz, P., Horner, E., Li, N., Mason, S., Nel, A., Oullette, J., Reijula, K., Reponen, T., Seltzer, J., Smith, A., and Tarlo, S. M.: The health effects of nonindustrial indoor air pollution, J. Allergy Clin. Immun., 121, 585–591, doi:10.1016/j.jaci.2007.10.045, 2008.

Bur, C., Reimann, P., Andersson, M., Schütze, A., and Lloyd Spetz, A.: Increasing the Selectivity of Pt-Gate SiC Field Effect Gas Sensors by DynamicTemperature Modulation, IEEE Sens. J., 12, 1906–1913, doi:10.1109/JSEN.2011.2179645, 2012.

Bur, C., Bastuck, M., Lloyd Spetz, A., Andersson, M., and Schütze, A.: Selectivity enhancement of SiC-FET gas sensors by combining temperature and gate bias cycled operation using multivariate statistics, Sensor. Actuat. B-Chem., 193, 931–940, doi:10.1016/j.snb.2013.12.030, 2014.

Caricato, A. P., Luches, A., and Rella, R.: Nanoparticle thin films for gas sensors prepared by matrix assisted pulsed laser evaporation, Sensors, 9, 2682–2696, doi:10.3390/s90402682, 2009.

European Parliament, Council of the European Union: Directive 2008/50/EC of the European Parliament and of the Council of 21 May 2008 on ambient air quality and cleaner air for Europe, Official Journal of the European Union, 51, 2008.

Gramm, A. and Schütze, A.: High performance solvent vapor identification with a two sensor array using temperature cycling and pattern classification, Sensor. Actuat. B-Chem., 95, 58–65, doi:10.1016/S0925-4005(03)00404-0, 2003.

Guo, H., Lee, S. C., Chan, L. Y., and Li, W. M.: Risk assessment of exposure to volatile organic compounds in different indoor environments, Environ. Res., 94, 57–66, doi:10.1016/S0013-9351(03)00035-5, 2004.

Gutierrez-Osuna, R.: Pattern Analysis for machine olfaction: A review, IEEE Sens. J., 2, 189–202, doi:10.1109/JSEN.2002.800688, 2002.

Harilal, S. S., Bindhu, C. V., Tillack, M. S., Najmabadi, F., and Gaeris, A. C.: Internal structure and expansion dynamics of laser ablation plumes into ambient gases, J. Appl. Phys., 93, 2380–2388, doi:10.1063/1.1544070, 2003.

Heilig, A., Bârsan, N., Weimar, U., Schweizer-Berberich, M., Gardner, J. W., and Göpel, W.: Gas identification by modulating temperatures of SnO_2-based thick film sensors, Sensor. Actuat. B-Chem., 43, 45–51, doi:10.1016/S0925-4005(97)00096-8, 1997.

Helwig, N., Schüler, M., Bur, C., Schütze, A., and Sauerwald, T.: Gas mixing apparatus for automated gas sensor characterization, Meas. Sci. Technol., 25, 055903, doi:10.1088/0957-0233/25/5/055903, 2014.

Huotari, J., Lappalainen, J., Puustinen, J., Baur, T., Alépée, C., Haapalainen, T., Komulainen, S., Pylvänäinen, J., and Lloyd Spetz, A.: Pulsed laser deposition of metal oxide nanoparticles, agglomerates, and nanotrees for chemical sensors, Procedia Eng., 120, 1158–1161, doi:10.1016/j.proeng.2015.08.745, 2015.

Hussain, O. M., Swapnasmitha, A. S., John, J., and Pinto, R.: Structure and morphology of laser-ablated WO_3 thin films, Appl. Phys. A, 81, 1291–1297, 2005.

Infortuna, I., Harvey, A. S., and Gauckler, L. J.: Microstructures of CGO and YSZ thin films by pulsed laser deposition, Adv. Funct. Mater., 18, 127–135, doi:10.1007/s00339-004-3041-z, 2008.

Johansson, M. B., Niklasson, G. A., and Österlund, L.: Structural and optical properties of visible active photocatalytic WO_3 thin films prepared by reactive dc magnetron sputtering, J. Mater. Res., 27, 3130–3140, doi:10.1557/jmr.2012.384, 2012.

Jones, A. P.: Indoor air quality and health, Atmos. Environ., 33, 4535–4564, doi:10.1016/S1352-2310(99)00272-1, 1999.

Klecka, W. R.: Discriminant Analysis, in: Quantitative applications in the social sciences, SAGE University Paper, 72 pp., 1980.

Kohl, D., Heinert, L., Bock, J., Hofmann, Th., and Schieberle, P.: Systematic studies on responses of metal-oxide sensor surfaces to straight chain alkanes, alcohols, aldehydes, ketones, acids and

esters using the SOMMSA approach, Sensor. Actuat. B-Chem., 70, 43–50, doi:10.1016/S0925-4005(00)00552-9, 2000.

Koistinen, K., Kotzias, D., Kephalopoulos, S., Schlitt, C., Carrer, P., Jantunen, M., Kirchner, S., McLaughlin, J., Mølhave, L., Fernandes, E. O., and Seifert, B.: The INDEX project: executive summary of a European Union project on indoor air pollutants, Allergy, 63, 810–819, doi:10.1111/j.1398-9995.2008.01740.x, 2008.

Lee, A. P. and Reedy, B. J.: Temperature modulation in semiconductor gas sensing, Sensor. Actuat. B-Chem., 60, 35–42, doi:10.1016/S0925-4005(99)00241-5, 1999.

Leidinger, M., Sauerwald, T., Reimringer, W., Ventura, G., and Schütze, A.: Selective detection of hazardous VOCs for indoor air quality applications using a virtual gas sensor array, J. Sens. Sens. Syst., 3, 253–263, doi:10.5194/jsss-3-253-2014, 2014.

Marinkovic, B., Ribeiro de Avillez, R., Saavedra, A., and Assunção, F. C. R.: A comparison between the Warren-Averbach method and alternate methods for x-ray diffraction microstructure analysis of polycrystalline specimens, Mat. Res., 4, 71–76, doi:10.1590/S1516-14392001000200005, 2001.

Meier, D. C., Evju, J. K., Boger, Z., Raman, B., Benkstein, K. D., Martinez, C. J., Montgomery, C. B., and Semancik, S.: The potential for and challenges of detecting chemical hazards with temperature-programmed microsensors, Sensor. Actuat. B-Chem., 121, 282–294, doi:10.1016/j.snb.2006.09.050, 2007.

Nam, H.-J., Sasaki, T., and Koshizaki, N.: Optical CO gas sensor using a cobalt oxide thin film prepared by pulsed laser deposition under various argon pressures, J. Phys. Chem. B, 110, 23081–23084, doi:10.1021/jp063484f,2006.

Paczkowski, S., Paczkowska, M., Dippel, S., Schulze, N., Schütz, S., Sauerwald, T., Weiß, A., Bauer, M., Gottschald, J., and Kohl, C.-D.: The olfaction of a fire beetle leads to new concepts for early fire warning systems, Sensor. Actuat. B-Chem., 183, 273–282, doi:10.1016/j.snb.2013.03.123, 2013.

Pihosh, Y., Turkevych, I., Mawatari, K., Uemura, J., Kazoe, Y., Kosar, S., Makita, K., Sugaya, T., Matsui, T., Fujita, D., Tosa, M., Kondo, M., and Kitamori, T.: Photocatalytic generation of hydrogen by core-shell WO_3/$BiVO_4$ nanorods with ultimate water splitting efficiency, Sci. Rep., 5, 11141, doi:10.1038/srep11141, 2015.

Reimann, P. and Schütze, A.: Fire detection in coal mines based on semiconductor gas sensors, Sensor Rev., 32, 47–58, doi:10.1108/02602281211197143, 2012.

Righettoni, M., Tricoli, A., and Pratsinis, S: $Si:WO_3$ Sensors for Highly Selective Detection of Acetone for Easy Diagnosis of Diabetes by Breath Analysis, Anal. Chem., 82, 3581–3587, doi:10.1021/ac902695n, 2010.

Sauerwald, T.: Nachweis von Luftschadstoffen mit Halbleiter-Gassensoren – Möglichkeiten und Einschränkungen, VDI-Berichte 2011, VDI Verlag GmbH, Düsseldorf, 2008.

Sood, S. and Gouma, P.-I.: Polymorphism in nanocrystalline binary metal oxides, Nanomater. Energy, 2, 82–96, 2013.

Souza Filho, A. G., Freire, P. T. C., Pilla, O., Ayala, A. P., Mendes Filho, J., Melo, F. E. A., Freire, V. N., and Lemos, V.: Pressure effects in the Raman spectrum of WO_3 microcrystals, Phys. Rev. B., 62, 3699–3703, doi:10.1103/PhysRevB.62.3699, 2000.

Wang, L., Teleke, A., Pratsinis, S. E., and Gouma, P.-I.: Ferroelectric WO_3 nanoparticles for acetone selective detection, Chem. Mater., 20, 4794–4796, doi:10.1021/cm800761e, 2008.

World Health Organization: WHO Guidelines for Indoor Air Quality: Selected Pollutants, Geneva, 2010.

Wu, C.-H., Feng, C.-T., Lo, Y.-S., Lin, T.-Y., and Lo, J.-G.: Determination of volatile organic compounds in workplace air by multisorbent adsorption/thermal desorption-GC/MS, Chemosphere, 56, 71–80, doi:10.1016/j.chemosphere.2004.02.003, 2004.

Zheng, H., Zhen Ou, J., Strano, M. S., Kaner, R. B., Mitchell, A., and Kalantar-zadeh, K.: Nanostructured tungsten oxide – Properties, synthesis, and applications, Adv. Funct. Mater., 21, 2175–2196, doi:10.1002/adfm.201002477, 2011.